Received: 4 December 2016 | Revised: 4 May 2017 | Accepted: 7 May 2017

DOI: 10.1111/gcb.13775

PRIMARY RESEARCH ARTICLE

WILEY Global Change Biology

Measuring canopy loss and climatic thresholds from an extreme drought along a fivefold precipitation gradient across Texas

Amanda M. Schwantes[1] | Jennifer J. Swenson[1] | Mariano González-Roglich[1,2] | Daniel M. Johnson[1,3] | Jean-Christophe Domec[1,4] | Robert B. Jackson[1,5]

[1]Nicholas School of the Environment, Duke University, Durham, NC, USA

[2]Conservation International, Arlington, VA, USA

[3]Department of Forest, Rangeland, and Fire Sciences, University of Idaho, Moscow, ID, USA

[4]Bordeaux Sciences Agro, UMR INRA-ISPA 1391, Gradignan, France

[5]Department of Earth System Science, Woods Institute for the Environment, and Precourt Institute for Energy, Stanford University, Stanford, CA, USA

Correspondence
Amanda M. Schwantes, Nicholas School of the Environment, Duke University, Durham, NC, USA.
Email: amanda.schwantes@duke.edu

Funding information
National Aeronautics and Space Administration, Grant/Award Number: Earth and Space Science Fellowship (NNX13AN86H); National Institute of Food and Agriculture, Grant/Award Number: 2012-68002-19795

Abstract

Globally, trees are increasingly dying from extreme drought, a trend that is expected to increase with climate change. Loss of trees has significant ecological, biophysical, and biogeochemical consequences. In 2011, a record drought caused widespread tree mortality in Texas. Using remotely sensed imagery, we quantified canopy loss during and after the drought across the state at 30-m spatial resolution, from the eastern pine/hardwood forests to the western shrublands, a region that includes the boundaries of many species ranges. Canopy loss observations in ~200 multitemporal fine-scale orthophotos (1-m) were used to train coarser Landsat imagery (30-m) to create 30-m binary statewide canopy loss maps. We found that canopy loss occurred across all major ecoregions of Texas, with an average loss of 9.5%. The drought had the highest impact in post oak woodlands, pinyon-juniper shrublands and Ashe juniper woodlands. Focusing on a 100-km by ~1,000-km transect spanning the State's fivefold east–west precipitation gradient (~1,500 to ~300 mm), we compared spatially explicit 2011 climatic anomalies to our canopy loss maps. Much of the canopy loss occurred in areas that passed specific climatic thresholds: warm season anomalies in mean temperature (+1.6°C) and vapor pressure deficit (VPD, +0.66 kPa), annual percent deviation in precipitation (−38%), and 2011 difference between precipitation and potential evapotranspiration (−1,206 mm). Although similarly low precipitation occurred during the landmark 1950s drought, the VPD and temperature anomalies observed in 2011 were even greater. Furthermore, future climate data under the representative concentration pathway 8.5 trajectory project that average values will surpass the 2011 VPD anomaly during the 2070–2099 period and the temperature anomaly during the 2040–2099 period. Identifying vulnerable ecological systems to drought stress and climate thresholds associated with canopy loss will aid in predicting how forests will respond to a changing climate and how ecological landscapes will change in the near term.

KEYWORDS

change detection, climate change, disturbance, extreme event, forest die-off, random forests, tree mortality, vapor pressure deficit

1 | INTRODUCTION

As climate change progresses, droughts in many areas are expected to increase in severity, duration, and frequency and, as a result, forests will likely become more vulnerable to drought-induced tree mortality (Allen, Breshears, & McDowell, 2015). Already, tree mortality events have been observed across the globe (Allen et al., 2010), ranging from increases in background mortality rates (van Mantgem et al., 2009) to regional die-offs (Breshears et al., 2005). As temperature extremes become more common under climate change, the likelihood of droughts occurring simultaneously with heatwaves is increasing (AghaKouchak, Cheng, Mazdiyasni, & Farahmand, 2014). These 'hotter droughts' can be particularly destructive to forests by increasing respiration and, in consequence, the potential for carbon starvation; increasing water stress due to rising atmospheric moisture demand could also result in hydraulic failure (Allen et al., 2015). Increased tree mortality will affect many critical factors, including impacts to community composition (Mueller et al., 2005), food webs (Carnicer et al., 2011), biophysics (Jackson et al., 2008; Rotenberg & Yakir, 2010), carbon cycling (Ciais et al., 2005; Michaelian, Hogg, Hall, & Arsenault, 2011), ecohydrology (Adams et al., 2012), stream flow (Guardiola-Claramonte et al., 2011), and phenology (Ivits, Horion, Fensholt, & Cherlet, 2014). Forests provide important ecosystem services; however, their fate under a changing climate with increased drought and heatwaves is uncertain.

To improve forecasts of how forests will respond to climate change, quantitative relationships between tree mortality and climate are needed, even if these relationships are empirical (Adams et al., 2013). Until the mechanisms surrounding tree death are well understood and enough data exist to parameterize global vegetation models, empirical relationships may represent the most appropriate avenue for forecasting tree mortality (Adams et al., 2013). Tree mortality is often linked to reduced precipitation, increased temperature, and associated increased vapor pressure deficit (VPD) (Allen et al., 2015). VPD is defined as the difference between saturated vapor pressure and actual vapor pressure and is largely dependent on temperature. Other drought indices have been proposed that incorporate both precipitation and temperature. For example, the difference between precipitation and potential evapotranspiration, P-PET, accounts for both supply and atmospheric moisture demand (Rind, Goldberg, Hansen, Rosenzweig, & Ruedy, 1990). A water deficit occurs on the landscape when precipitation is less than potential evapotranspiration and P-PET is negative. Furthermore, tree mortality often has a threshold response with climate (Clifford, Royer, Cobb, Breshears, & Ford, 2013). Once a specific climatic anomaly is surpassed, the likelihood of tree mortality increases substantially.

Many studies have linked mortality events to climatic anomalies. These studies include tree-ring analysis to develop a forest drought stress index in the southwest United States (Williams et al., 2013) as well as field surveys in Amazonia and Borneo (Phillips et al., 2010) and in Australia (Mitchell, O'Grady, Hayes, & Pinkard, 2014). However, fewer studies have examined relationships between remotely sensed observations of tree mortality across climatic gradients. For example, precipitation and VPD thresholds were related to pinyon pine (*Pinus edulis*) mortality for a sub region of New Mexico (Clifford et al., 2013), and climatic water deficit was linked to aspen (*Populus tremuloides*) mortality in a part of Colorado (Anderegg et al., 2015). Such studies focused on one natural system with only a couple of dominant tree species. In this study, we examine remotely sensed observations of tree mortality across a much larger climatic gradient from humid to semiarid regions. Through remote sensing, climate can be linked to continuous spatially explicit estimates of tree mortality across large areas, closer to the extent of regional vegetation models.

Remote sensing approaches tailored specifically for drought-induced tree mortality that can span large areas at a fine resolution are also needed. Tree mortality caused by drought is often an irregular process by which some individuals die but neighboring trees remain alive. Dead trees scattered among many live trees are more difficult to quantify using remote sensing approaches compared to disturbances that kill entire stands (McDowell et al., 2015). At coarser scales, pixels are often 'mixed', containing multiple cover types (i.e., canopy loss and live canopy) and there may be excess zero pixels (i.e., homogenous live canopy cover), if low-levels of mortality occur. Many remote sensing techniques have been proposed to quantify drought-induced tree mortality, including spectral mixture analysis (Huang & Anderegg, 2012), zero-inflated models (Schwantes, Swenson, & Jackson, 2016), and time-series of spectral indices (Vogelmann, Tolk, & Zhu, 2009; Meddens, Hicke, Vierling, & Hudak, 2013). However, these studies were designed for mapping mortality in only one natural system with a few dominant species. Other studies have proposed techniques that work across systems using Moderate Resolution Imaging Spectroradiometer (MODIS), such as the MODIS global disturbance index (Mildrexler, Zhao, & Running, 2009) and the ForWarn system (Norman, Koch, & Hargrove, 2016). However, the spatial resolution of these products ranges from 250 m to 1 km, which is too coarse to capture local-scale disturbances (McDowell et al., 2015). Alternatively, the 30-m resolution of Landsat imagery is a more appropriate scale to detect forest cover changes (Cohen & Goward, 2004). In this study, we implement a remote sensing approach that (i) maps canopy loss across diverse ecoregions at regional scales and (ii) accommodates excess zeros and mixed pixels, inherent to disturbances like drought-induced tree mortality.

Texas was advantageous for studying drought-induced tree mortality because it was the location of an extreme drought and heat wave in 2011 and it spans a large climatic gradient from humid to semiarid regions. Using statewide averages of Palmer Drought Severity Index (PDSI) data from 1895 to 2011, Hoerling et al. (2013) found that the 2011 drought reached a record statewide minimum PDSI of −7.93. The 2011 drought was also the driest 12-month period, October 2010 to September 2011, on record (Hoerling et al., 2013). Furthermore, due to low atmospheric moisture and high temperatures, the 2011 drought was also associated with a record high VPD (Williams et al., 2014). Although it is challenging to definitively link episodic climatic events to climate change, models indicate that

abnormally high summer temperatures in Texas are increasing in likelihood (Rupp et al., 2015). Furthermore, in the southwestern United States, temperature and VPD are projected to increase in the future (Williams et al., 2014). Texas has over 200 ecological plant community types dominated by woody species (Elliott et al., 2014), spanning a broad range of annual precipitation regimes from humid to semiarid. As such, Texas contains the most arid edge of many species' ranges (e.g., the eastern hardwoods). These trailing range edges often see heightened drought-induced tree mortality (Jump, Mátyás, & Peñuelas, 2009).

In this study, we identify empirical relationships between climate and canopy loss observed during and after the drought and determine if, and when, the 2011 climatic anomalies are projected to be crossed in the future. To detect canopy loss from the 2011 drought across Texas, we first created a multitemporal training dataset by classifying 194 fine-scale 1-m orthophoto sets (Schwantes et al., 2016). We then used random forests models to relate the canopy loss observed in the 1-m orthophoto classifications to 30-m Landsat imagery to estimate drought impact across the state of Texas. These coarse-scale regional maps were used to identify ecological systems most impacted by the drought. We also identified threshold relationships between climate and spatial patterns of canopy loss across the fivefold precipitation gradient spanning humid to semiarid regions. Lastly, we examined whether the 2011 climate anomalies would likely be surpassed in the future using downscaled projected climate data, under representative concentration pathway, RCP, 4.5 and 8.5 trajectories.

2 | MATERIALS AND METHODS

2.1 | Study area

The state of Texas was selected because (i) it was the center of a major drought and tree mortality event in 2011, (ii) its natural precipitation gradient was large for areas dominated by tree cover, extending from mean annual precipitation (MAP) of ~1,500 mm in the east to ~300 mm in the west, and (iii) it included the edges of many species' ranges (e.g., eastern hardwoods such as *Quercus stellata* and many western shrubland species like *Juniperus ashei*). The 12 U.S. EPA level III ecoregions in the state of Texas followed the east–west precipitation gradient, transitioning from dense closed-canopy forests to the open-canopy savannas to the western shrublands (Table 1). We excluded the high plains in this study, because the area was dominated by grasslands, with little or no woody plant cover. We divided our study area into six zones for purposes of modeling by combining the 11 ecoregions into zones based on similar species and climate: (i) Pineywoods, (ii) Oakwoods/Blackland Prairies, (iii) Rolling Plains, (iv) Edwards Plateau, (v) South Texas, and (vi) Trans Pecos (Figure 1, Table 1). A decrease in precipitation and an increase in mean temperature compared to historical averages were observed during the 2011 drought across all six modeling zones (Table 1; PRISM Climate Group, 2015). Moreover, precipitation decreased by more than half of the historical average for the Trans Pecos and Edwards Plateau.

2.2 | Creating training and testing data: classification and field validation of 1-m canopy loss maps

Following Schwantes et al. (2016), we created a training and testing dataset of fine-scale canopy loss maps, from supervised classifications of stacks of predrought (2010) and postdrought (2012) orthophotos from the National Agriculture Imagery Program (NAIP) (US Department of Agriculture, 2014). The 1-m orthophotos (four bands: red, green, blue, near-infrared, NIR) were flown during the growing season, were already orthorectified to true ground, errors within 6 m, and were tiled based on quarter quads, each ~41 km^2. We randomly selected 186 NAIP quarter quads using a blocked random sample, where blocks were the Landsat footprints (each ~23,000 km^2), excluding areas of overlapping Landsat scenes. The number of NAIP quarter quads chosen per Landsat footprint was weighted by the forest-area proportion in the Landsat footprint. We

TABLE 1 Climate data (historical averages and 2011 values) for the six modeling zones

		Spatial mean of annual precipitation (mm)		Spatial mean of warm season mean temp (°C)	
Modeling zone	Level III ecoregions (U.S. EPA)	Hist. mean ± *SD*[a]	2011 mean	Hist. mean ± *SD*[a]	2011 mean
1. Pineywoods	• South Central Plains	1222 ± 228	826	25.9 ± 0.7	28.1
2. Oakwoods & Blackland Prairies	• Texas Blackland Prairies • East Central Texas Plains	948 ± 195	608	26.6 ± 0.7	28.6
3. Rolling Plains	• Southwestern Tablelands • Central Great Plains • Cross Timbers	646 ± 124	380	25.5 ± 0.8	28.0
4. Trans Pecos	• Arizona/New Mexico Mountains • Chihuahuan Deserts	317 ± 100	110	25.0 ± 0.7	27.1
5. Edwards Plateau	• Edwards Plateau	614 ± 150	295	25.7 ± 0.7	27.7
6. South Texas & Gulf Coast	• Southern Texas Plains • Western Gulf Coastal Plain	767 ± 172	384	27.9 ± 0.6	29.3

[a]The historical mean and standard deviation as calculated for years 1950 to 2005, using PRISM data (PRISM Climate Group, 2015).

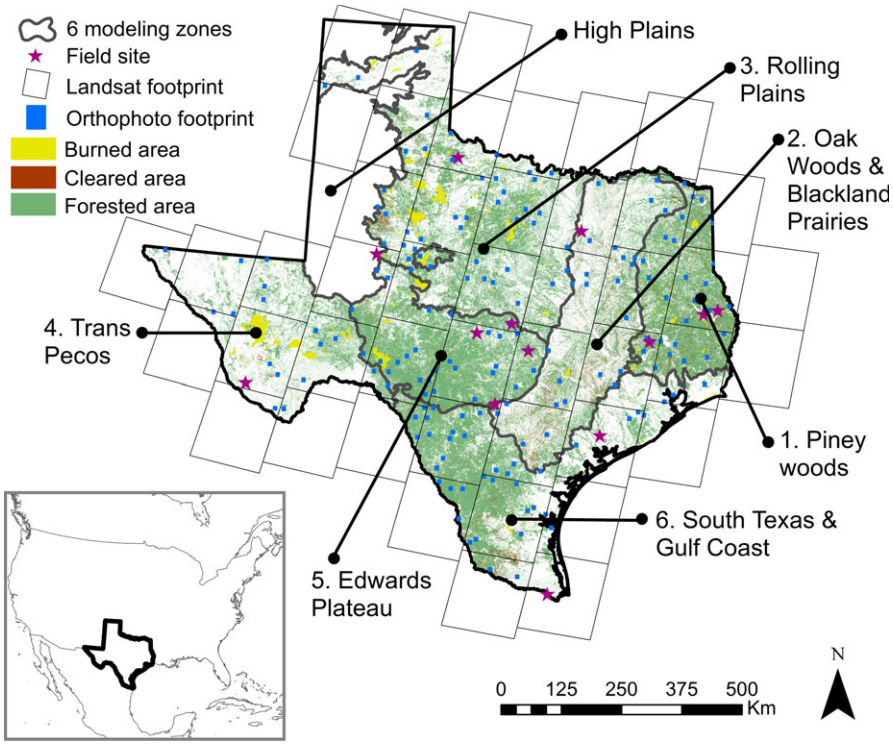

FIGURE 1 Modeling zones of Texas characterized as temperate deciduous forest, grassland, and desert biomes. The High Plains, nonforested, burned, and cleared areas were excluded from the analysis. We estimated canopy loss across three scales: field estimates of canopy loss (67 plots) were used to validate the fine-scale canopy loss maps derived from 1-m orthophotos (n = 194 at ~41 km^2 each), which were used to scale up to Landsat (46 footprints covering Texas, ~600,000 km^2)

selected an additional eight orthophotos nonrandomly based on access to public land, for the purpose of field validation; field access was limited in Texas.

For validation, we compared observations of canopy loss in the 1-m orthophoto classifications to measurements of dead and live crowns taken on the ground, following Schwantes et al. (2016). From July to Sept 2013 and during July 2014, we measured dead and live crowns in 13 sites (Figure 1), with 3–7 plots per site (Table S1), for a total of 67 plots. For each plot, we measured dead and live crowns (to the nearest 0.1-m) along four 25-m transects running from the randomized plot center to the plot edge following the four cardinal directions. All woody species >1-m in height were counted that intersected the transect. Rules for assigning the health status to each individual tree (e.g., dead, live, dead prior to drought) were outlined in Table S2. Canopy cover loss measurements of the uppermost layer of canopy, from each of the four transects, were summed for each plot, and compared to the total canopy loss observed in the orthophoto classifications, as estimated within a 25-m radius circular buffer from plot center. Further details on classification and validation of the orthophotos are described in Schwantes et al. (2016) and the supporting information.

2.3 | Scaling up to regional estimates using random forests: 30-m binary canopy loss map

To focus our analysis within forested regions and avoid misclassifications associated with fires and clearing, we excluded areas that were nonforest, burned, or cleared. We created a binary forest cover mask by including only ecological systems dominated by tree species (Elliott et al., 2014). Using data from the Monitoring Trends in Burn Severity project (USDA Forest Service/U.S. Geological Survey, 2014), we also excluded all areas that were burned from May 2009 to Oct 2014. Lastly, through visual inspection we used a band difference between postdrought and predrought tassel cap brightness bands (Crist, 1985; Baig, Zhang, Shuai, & Tong, 2014) of 0.1 to remove trees that were cleared in the Pineywoods and Oakwoods/Blackland Prairies and 0.2 for the four remaining western modeling zones.

Atmospherically corrected imagery from the Landsat surface reflectance product (Masek et al., 2006) was acquired from May to Oct with a preference for late summer images. Predrought images were either taken in 2009 or 2010 from the Landsat 5 TM archive. Landsat 5 TM became nonoperational Nov 2011, and Landsat 8 OLI, launched Feb 2013; therefore postdrought images were from the Landsat 8 OLI archive, 2–3 years after the drought (2013 or 2014; see Table S3 for acquisition dates). We manually co-registered NAIP images that showed poor alignment with Landsat scenes to achieve an RMSE <0.5 of a 30-m Landsat pixel.

To scale up from the 1-m orthophoto classifications to the 30-m Landsat imagery, we used random forests models (Breiman, 2001; Liaw & Wiener, 2002) in classification mode to create 30-m binary maps (loss or no loss) across Texas. Using a separate model for each of the six modeling zones, we employed random forests, a machine learning algorithm that created an ensemble of decision trees. Each decision tree was grown using a sample of the data and a subset of the explanatory variables. The nodes on each decision tree were created by splitting the explanatory variables in a way that created the most homogenous groups, until a minimum/terminal node size was reached. Bootstrap samples were taken with replacement to

build each decision tree; data withheld were used to compute the out-of-bag (OOB) error rate (Breiman, 2001). We did not find that our models were sensitive to parameterization; therefore, we used the following: 1001 decision trees, a node size of 1, and the number of variables used to build each decision tree equal to the square root of the total number of variables. By overlaying a grid at the spatial resolution of Landsat (30-m) onto the 1-m orthophoto classifications, we extracted proportion canopy loss for each 30-m grid cell and created a binary response variable for the random forests models: (i) pixels with zero canopy loss (no loss pixels with homogenous live canopy) and (ii) pixels with greater than 25% canopy loss (loss pixels). The explanatory variables for the random forests models were percent tree cover from the National Land Cover Databases (NLCD) (Homer et al., 2015) and 13 vegetation indices derived from Landsat (Table 2) for both pre and postdrought images. For variable selection, we created parsimonious models by removing variables that were highly correlated to greater than |0.95|. The final variables selected for each random forests model can be found in Table S4.

Much of the landscape experienced no mortality; thus, the canopy loss dataset contained many more pixels with zero canopy loss compared to pixels with greater than 25% canopy loss, and therefore, to improve the random forests model fits we made the following modifications. Firstly, we sampled each class equally for each decision tree in the random forests. Secondly, using random forests model outputs of the probability of a pixel's class membership, we tuned the models with receiver operating characteristic (ROC) curves (Sing, Sander, Beerenwinkel, & Lengauer, 2005). To determine the class of each pixel (e.g., canopy loss vs. no loss), we balanced true positive rate (TPR, accurately predicting a loss pixel when a loss pixel occurred) and true negative rate (TNR, accurately predicting a no loss pixel when no loss pixel occurred). Finally, to remove the influence of slight atmospheric differences between Landsat scenes, the random forests model was first run using all data within the modeling zone. Then, unique probability thresholds were chosen using the ROC analysis based on groups of Landsat footprints. Groups were chosen to match rows with similar acquisition dates or for individual Landsat scenes that had unique acquisition dates. The cutoff values used to define a loss pixel from a no loss pixel can be found in Table S5 and a more detailed explanation of the ROC analysis can be found in the supporting information.

TABLE 2 Landsat vegetation indices and auxiliary explanatory variables considered in random forests models

	Covariate	Citation
1	Difference vegetation index (DVI)	Tucker (1979)
2	Greenness normalized difference vegetation index (GNDVI)	Gitelson, Kaufman, and Merzlyak (1996)
3	Modified soil adjusted vegetation index (MSAVI)	Qi, Chehbouni, Huete, Kerr, and Sorooshian (1994)
4,5	Normalized burn ratio (NBR) Normalized burn ratio II (NBR2)	van Wagtendonk, Root, and Key (2004)
6	Normalized difference water index (NDWI)	Wilson and Sader (2002)
7	Normalized difference vegetation index (NDVI)	Tucker (1979)
8	Ratio SWIR/NIR	Vogelmann and Rock (1988)
9	Red green index (RGI)	Coops, Johnson, Wulder, and White (2006)
10	Soil adjusted vegetation index (SAVI)	Huete (1988)
11,12,13	Tasseled cap brightness (TCB), greenness (TCG), wetness (TCW)	Crist (1985) and Baig et al. (2014)
14	Percent tree cover (% tree)	Homer et al. (2015)

Not every pixel contained 100% canopy loss, and therefore to estimate the overall percent canopy loss, we multiplied the proportion of impacted 30-m pixels by the average canopy loss within each of the impacted pixels, as estimated using the 1-m orthophoto classifications for each modeling zone. We used the same procedure to compute overall relative canopy loss, defined as canopy loss divided by the live predrought canopy cover. In this way, we could more precisely determine the percent of forest impacted by the drought. To test model performance, we used spatially independent testing data, which provided a better estimate of the true mapping accuracy (González-Roglich & Swenson, 2016; Schwantes et al., 2016), by conducting leave-one-out cross validation for each orthophoto, independently for each of the six modeling zones (see supporting information for a complete description). As is the case for most remote sensing studies, we were only mapping aerial cover, defined as the uppermost layer of canopy (Fehmi, 2010); we were not mapping overlapping canopy cover. For example, if the overstory died and the midstory or understory remained alive, we would still consider this canopy loss. Moreover, analysis relying on remotely sensed imagery detects changes in canopy; therefore, we used the terms canopy loss and live canopy instead of dead and live trees. Image processing for the coarse-scale maps was completed in ENVI/IDL 5.0, ArcMap 10.3.1, Python 2.7.8, and R v. 3.1.3 (R Core Team, 2015).

2.4 | Defining relationships between spatial patterns of canopy loss and climate

To examine how climate drove the spatial patterning of canopy loss across a landscape, we used 4-km spatially interpolated climate data from PRISM (PRISM Climate Group, 2015). For each 4-km cell, we first calculated the relative canopy loss, defined as the number of 30-m drought-impacted pixels divided by the number of forest cover pixels. We then examined how four climate variables: annual precipitation, warm season (May–Sept) mean temperature, warm season VPD, and annual 2011 P-PET controlled mortality patterns across an east–west transect that was 100 km wide by ~1,000 km in length. In selecting the transect, we chose the widest horizontal swath across Texas that encompassed the greatest amount of ecosystem diversity.

As the transect spans a precipitation gradient, we calculated percent deviations from historical values for precipitation; however, for temperature and VPD we calculated anomalies, and for P-PET we used the 2011 value. The analysis was conducted on a sample of 20% of the 4-km pixels within the transect, excluding adjacent pixels with a minimum distance between cell centers of <8 km. We also only included pixels with >50% forested area to focus the analysis in predominantly forested regions. Precipitation and mean temperature were directly acquired (PRISM Climate Group, 2015), and daily VPD was calculated using mean temperature and dew point temperature following Daly, Smith, and Olson (2015). PET was acquired from GRIDMET, a 4-km gridded climate dataset, where PET was calculated using Penman-Monteith (Abatzoglou, 2013).

We identified climatic thresholds that when surpassed were associated with greater canopy loss, based on the first split in regression trees (Therneau, Atkinson, & Ripley, 2015). In this case, the numeric response variable was relative canopy loss within a 4-km pixel and the continuous explanatory variable was percent deviation or anomaly from normal climate. For each climate variable, the regression tree selected a breakpoint along the continuous climate variable that created the most homogenous response group (De'ath & Fabricius, 2000). In this way, climatic conditions associated with large amounts of canopy loss were differentiated from climates associated with little canopy loss. The breakpoint between these two groups was considered the climatic threshold that when crossed led to enhanced mortality. These climatic thresholds were identified across space; therefore, to further validate whether these thresholds could also hold true through time, we examined past climate from 1950 to 2015, using data from PRISM (PRISM Climate Group, 2015); however, PET data were only available from 1979 onwards (Abatzoglou, 2013).

2.5 | Projecting whether 2011 climate anomalies were likely to be crossed in the future

We determined whether the climate thresholds associated with canopy loss in 2011 were likely to be crossed in the future. Firstly, we acquired 4-km projected climate data, where statistical downscaling had been performed using the multivariate adapted constructed analogs (MACA) approach (Abatzoglou & Brown, 2012). Precipitation, temperature, and PET were acquired directly (Abatzoglou & Brown, 2012), whereas daily VPD was computed using mean temperature and specific humidity (Ross & Elliot, 1996). We examined the mean, standard deviation, and range of 20 global climate models (GCMs), using Coupled Model Intercomparison Project Phase 5 (CMIP5) results, under the Representative Concentration Pathway (RCP) 4.5 and 8.5 trajectories from 2006 to 2099 (Abatzoglou & Brown, 2012). Secondly to calculate historical values used to compute the anomalies from current climate, we used historical PRISM data (1950–2005); however, for calculating the historical values used to compute anomalies for future climate, we used historical projected MACA data (1950–2005). We only considered pixels with >50% forested area. Also, to further characterize the variability between the models, we estimated the percent of times that these climatic thresholds would be crossed over the latter half of the 21st century (2050–2099) across the 20 GCMs, creating spatially explicit maps for the state of Texas. For example, if 50% of the GCMs predicted that a threshold crossing would occur for 50% of the years from 2050 to 2099, then this would be represented by an average 25% times crossed.

2.6 | Identifying ecological systems most impacted by the 2011 drought

We determined which communities were most influenced by the 2011 drought through an overlay of our canopy loss maps and an ecological systems layer map (Elliott et al., 2014; Comer et al., 2003). We only considered ecological systems dominated by tree species, 231 systems, and then we further only included geographically dominant systems that covered at least 200 km^2, for a total of 94 systems. Of these 94 dominant systems, we present the top 10 most and least impacted, where the most impacted systems had the largest relative canopy loss defined as drought-impacted area divided by total area. The full analysis for all 231 tree-dominant systems can be found in Table S6.

3 | RESULTS

Ground estimates of canopy loss and postdrought live canopy cover were both highly correlated with the same attributes observed in the orthophoto classifications (R^2 = .82, RMSE = 4.7% for canopy loss; R^2 = .89 and RMSE = 11% for live canopy) (Figure 2). Overestimation of canopy cover loss in the orthophotos happened occasionally when trees lost most of their foliage and thus appeared dead in the orthophotos. Underestimates of tree cover loss occurred on occasion when dead trees were misclassified as alive, due to the presence of either dense understory shrubs or grass under the dead canopy, or extensive vines within the dead canopy.

In quantifying statewide 30-m binary canopy loss using random forests models, error rates and the covariates found to be the most important in predicting canopy loss were unique to each modeling zone. The normalized burn ratio and tassel cap brightness (TCB) indices were found to be the most important to modeling canopy loss in the Pineywoods region, whereas TCB, tassel cap wetness, and the difference vegetation index were the best predictors for the Trans Pecos and Edwards Plateau (Table S4). The out-of-bag (OOB) estimates of accuracy (ranging from 86% to 93%) were higher compared to the spatially independent estimates (ranging from 79% to 90%) (Table 3), likely because the latter were tested using spatially independent data. The spatially independent accuracy metric also reflects that the data had excess zeros, and as such the models tended to predict the common (no loss) pixels well (TNR), but the rarer class (loss pixels) less well (TPR). The model with the highest error was for the South Texas & Gulf Coast modeling zone (Table 3).

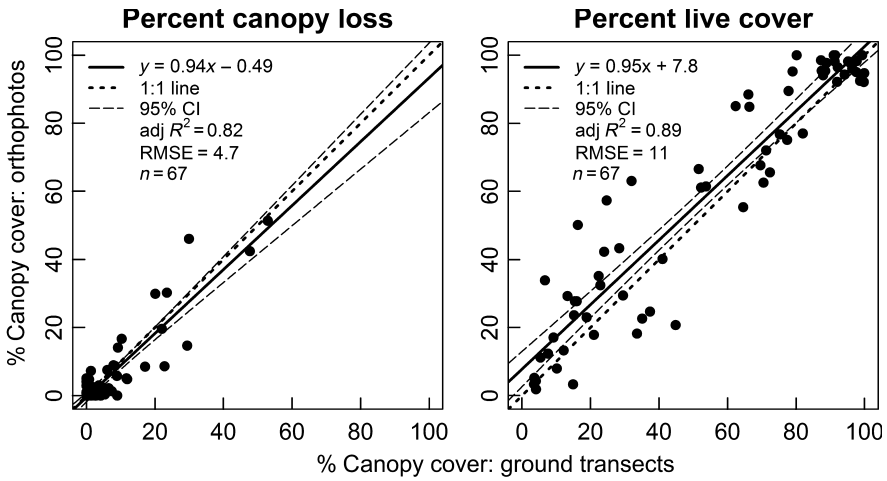

FIGURE 2 Field validation: canopy loss and live canopy cover measured using ground transects (2013–2014) compared to canopy loss and live canopy cover observed in the 1-m orthophoto classifications (imagery from 2010 and 2012)

TABLE 3 Accuracy of random forests models in distinguishing pixels of canopy loss (>25%) from pixels of no (0%) canopy loss

	Spatially independent			Final model (OOB)		
Modeling zone	% Accuracy	% TPR	% TNR	% Accuracy	% TPR	% TNR
Pineywoods	90	80	90	91	90	91
Oakwoods & Blackland Prairie	83	61	83	88	87	88
Rolling Plains	79	53	80	86	87	86
Trans Pecos	83	68	83	93	90	93
Edwards Plateau	84	81	85	91	91	91
South Texas & Gulf Coast	79	30	81	92	91	92

TPR, true positive rate (accurately predicting a loss pixel when a loss pixel occurred); TNR, true negative rate (accurately predicting a no loss pixel when a no loss pixel occurred).

Overall, 61,000 km^2 of forested area was impacted by the drought as defined by having >25% canopy loss per pixel (Figure 3, Table 4). Within forested pixels across the state, the drought caused an average 9.5% canopy loss and 15% relative canopy loss, defined as canopy cover loss divided by predrought live canopy cover (Table 4). Relative canopy loss was a more useful comparison metric considering that average predrought percent live canopy ranged from 21% in the Trans Pecos to 85% in the Pineywoods according to the orthophoto classifications. The Pineywoods region was the least impacted in terms of canopy loss and relative canopy loss. The other five western modeling zones were severely impacted by the drought when considering relative canopy loss.

Spatial patterns of canopy loss in Texas exhibited threshold responses with warm season VPD, warm season temperature, annual precipitation, and 2011 annual P-PET. When a climatic threshold was surpassed, more tree mortality occurred. A threshold response was apparent, where 4-km pixels had greater canopy loss with either a VPD anomaly greater than 0.66 kPa, a temperature anomaly greater than 1.6°C, a percent deviation in precipitation less than −38%, or a 2011 P-PET water deficit less than −1,206 mm (Figure 4).

To test whether the climatic thresholds we identified for 2011 occurred in the past, we used PRISM data from 1950 to 2015. The temperature threshold was only crossed twice, during 1998 and 2011 (Figure 5), whereas the VPD anomaly was only surpassed once, during the 2011 drought. The precipitation threshold was crossed twice (1950s and 2011) over the historical climate period. Precipitation levels in 2011 were similar to the 1950s drought; however, the 2011 drought was uniquely characterized by higher temperatures and VPDs.

The temperature threshold was projected to be surpassed on average for the two time periods: 2040–2069 and 2070–2099 (black diamonds in Figure 5), when considering an ensemble average across 20 GCMs, under RCP 4.5 and 8.5. However, the VPD anomaly and the 2011 P-PET water deficit were both projected to be surpassed on average only for the 2070–2099 period under the RCP 8.5 scenario. Conversely, the future precipitation projection ensemble mean did not project any crossings of these precipitation thresholds; however, the ensemble range and standard deviation did cross the threshold in the future.

The proportion of times and models for which a threshold was projected to be crossed varied across space and was unique to each climate variable, when considering 20 GCMs and a 50-year time-period, 2050–2099 (Figure 6). Although, the ensemble mean for precipitation was never projected to cross the precipitation threshold in the future, for portions of the landscape, precipitation thresholds were crossed 4%–16% (RCP 4.5) and 6%–20% (RCP 8.5) of the time for the latter half of the 21st century and across 20 GCMs. Thresholds were crossed more often for VPD ranging from 0% to 28% (RCP 4.5) and 0% to 62% (RCP 8.5) as well as for temperature ranging from 75% to 86% (RCP 4.5) and 96% to 98% (RCP 8.5) (Figure 6). P-PET threshold crossings ranged from 0% to 100% for both RCP 4.5 and 8.5 scenarios. The precipitation thresholds were projected to be crossed more frequently for Central and South Texas, for both RCP 4.5 and 8.5, and the southern edge of East Texas (Pineywoods) for RCP 8.5. For VPD under both

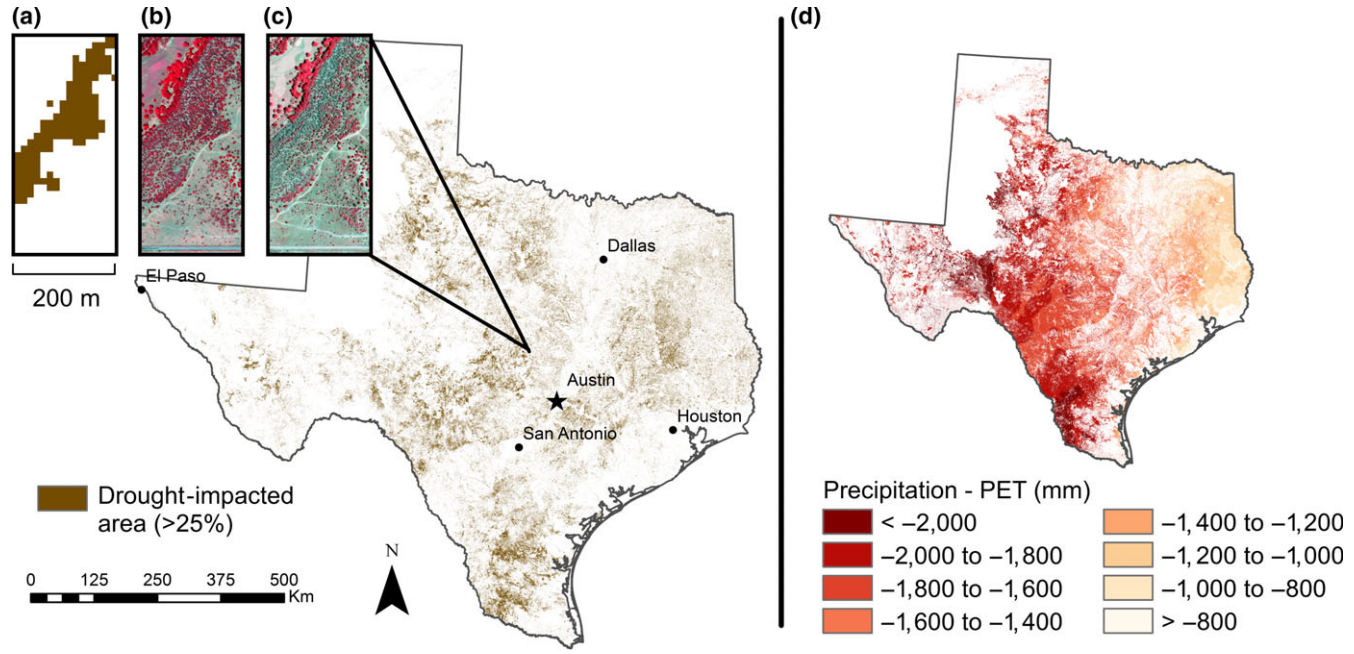

FIGURE 3 Drought-impacted area (>25% canopy loss per pixel) across Texas. Insets: an example near Lampasas of (a) 30-m binary canopy loss maps, (b) predrought 2010 orthophoto (1-m) and (c) postdrought 2012 orthophoto. On average, the 2011 drought caused 9.5% canopy loss (15% relative canopy loss) statewide within all forested pixels. (d) The difference between 2011 annual precipitation and potential evapotranspiration (PET) originally at a 4-km spatial resolution was resampled to 30-m to provide a direct comparison to the 30-m drought-impacted area maps

TABLE 4 Summary of percent forest cover lost and impacted area by modeling zone

Modeling zone	Estimated area impacted (km^2)	Avg. % canopy loss in loss pixels[a]	Avg. relative % canopy loss in loss pixels[b]	Overall avg. % canopy loss[c]	Overall avg. relative % canopy loss
Pineywoods	8,842	35	40	6.8	7.8
Oakwoods & Blackland Prairie	8,818	36	43	9.8	12
Rolling Plains	15,760	36	60	9.9	16
Trans Pecos	3,865	42	73	7.9	14
Edwards Plateau	11,522	39	65	8.8	15
South Texas & Gulf Coast	12,157	46	68	10	16
Total	60,969	41	63	9.5	15

[a,b]The average percent canopy loss (col 3) and relative percent canopy loss (col 4) per each loss pixel, according to the 1-m orthophoto classifications.
[c]The overall average percent canopy loss (col 5) was computed as the percent of the landscape experiencing loss multiplied by the average percent cover loss per loss pixel (col 3).

scenarios, and for temperature under RCP 4.5, thresholds were less likely to be crossed near the gulf coast; however, for RCP 8.5, the temperature threshold was crossed almost uninterruptedly for most of the region (Figure 6).

For the 94 ecological systems where trees were dominant and covered >200 km^2 in area, we present the top most and least impacted systems. Table S6 contains drought impacts for all 231 ecological systems dominated by tree species. The systems most negatively affected by the 2011 drought (Figure 7) were the pinyon-juniper (*Pinus cembroides*, *Juniperus deppeana*, *J. pinchotii*, and *J. flaccida*) and oak systems (*Quercus grisea*, *Q. emoryi*, *Q. hypoleucoides*, *Q. arizonica*, *Q. rugose*, and *Q. mohriana*) of the Trans Pecos, the post oak (*Q. stellata*) woodlands of the Llano uplift, and the juniper woodlands (*J. ashei*, *J. virginiana*, *J. monosperma* and *J. pinchotii*) of the Edwards Plateau (Moir, 1982; Elliott et al., 2014). Furthermore, systems on sandy sites (e.g., sandy mesquite evergreen woodlands and sandy shinnery shrublands) tended to have more canopy loss. Alternatively, systems in riparian and mesic areas as well as managed systems were less impacted. Lastly, communities dominated by the invasive Chinese Tallow (*Triadica sebifera L.*), had some of the lowest canopy loss.

4 | DISCUSSION

We mapped drought-induced canopy loss using a consistent method across a fivefold precipitation gradient that spanned humid to semiarid regions. We took advantage of open-source remotely sensed imagery at two spatial scales and new machine

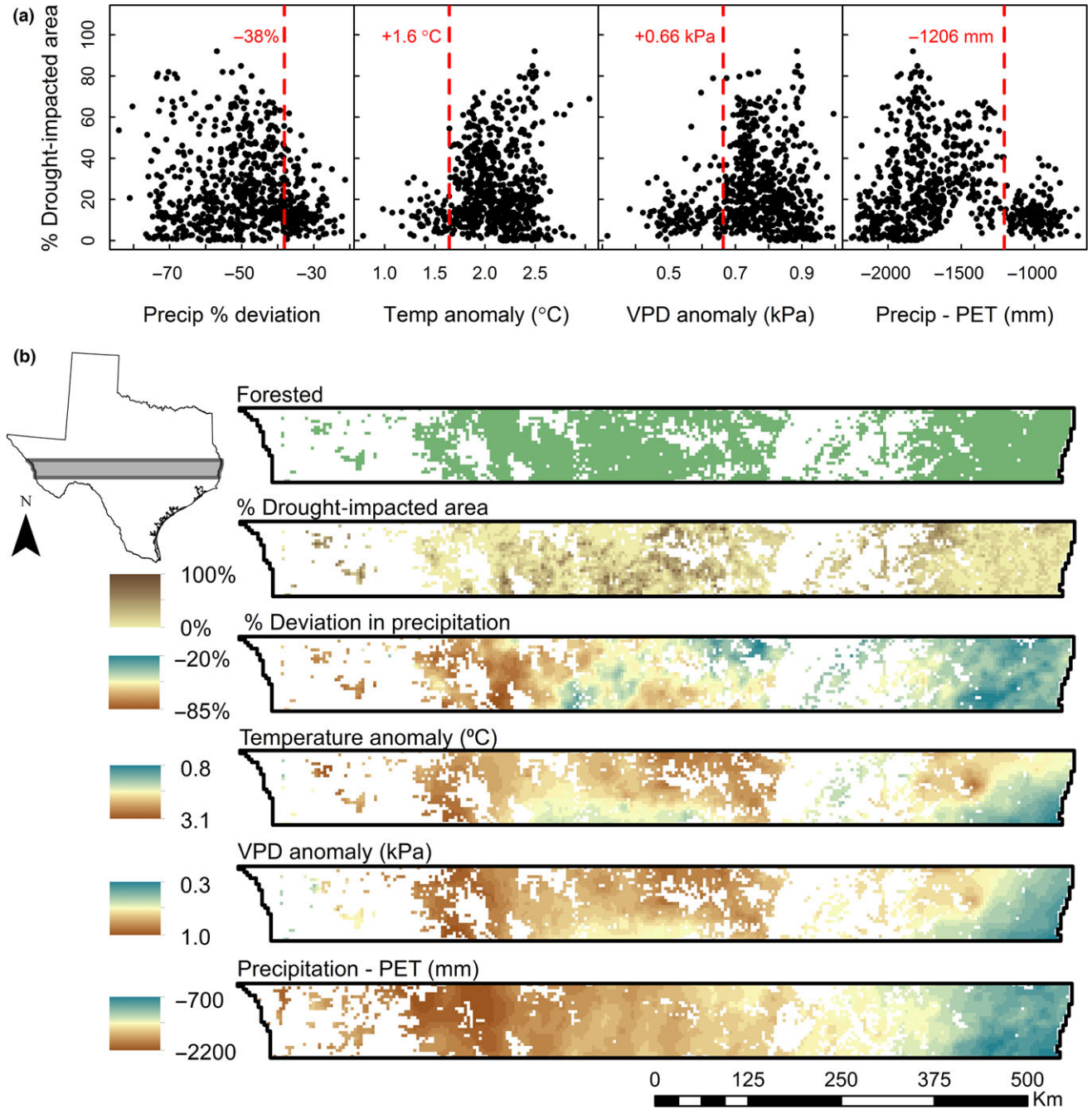

FIGURE 4 Climatic drivers of the spatial patterns of canopy loss across Texas. (a) Threshold values (red) for annual precipitation, warm season temperature, warm season vapor pressure deficit, VPD (PRISM Climate Group, 2015) and 2011 annual precipitation minus potential evapotranspiration, P-PET, (Abatzoglou, 2013). Positive anomalies for temperature and VPD indicate greater mortality, whereas negative values for precipitation and P-PET signify greater canopy loss. (b) Spatial comparison of climate to percent impacted area and forest cover (majority of 4-km pixel within forest cover mask), along the 100 km by ~1,000-km east-west transect. Data points (a) represent randomly selected 4-km pixels along the transect (b)

learning algorithms to create binary canopy loss maps. We then used these maps to identify climatic thresholds that explained spatial patterns of canopy loss and determined which ecological systems were most impacted and thus potentially more vulnerable to climate change.

Across Texas, we found 9.5% canopy loss resulting from the 2011 drought in a region that is vulnerable to ongoing climate shifts. Canopy loss occurred across all the ecoregions of Texas, with the western systems most impacted. The humid systems (e.g., Piney-woods and Oakwoods/Blackland Prairies) had less relative canopy loss, 8% and 12% respectively, compared to the other more arid western systems, all with greater than or equal to 14% relative canopy loss (Table 4). However, canopy loss occurred across the entire precipitation gradient, signifying that drought-induced tree

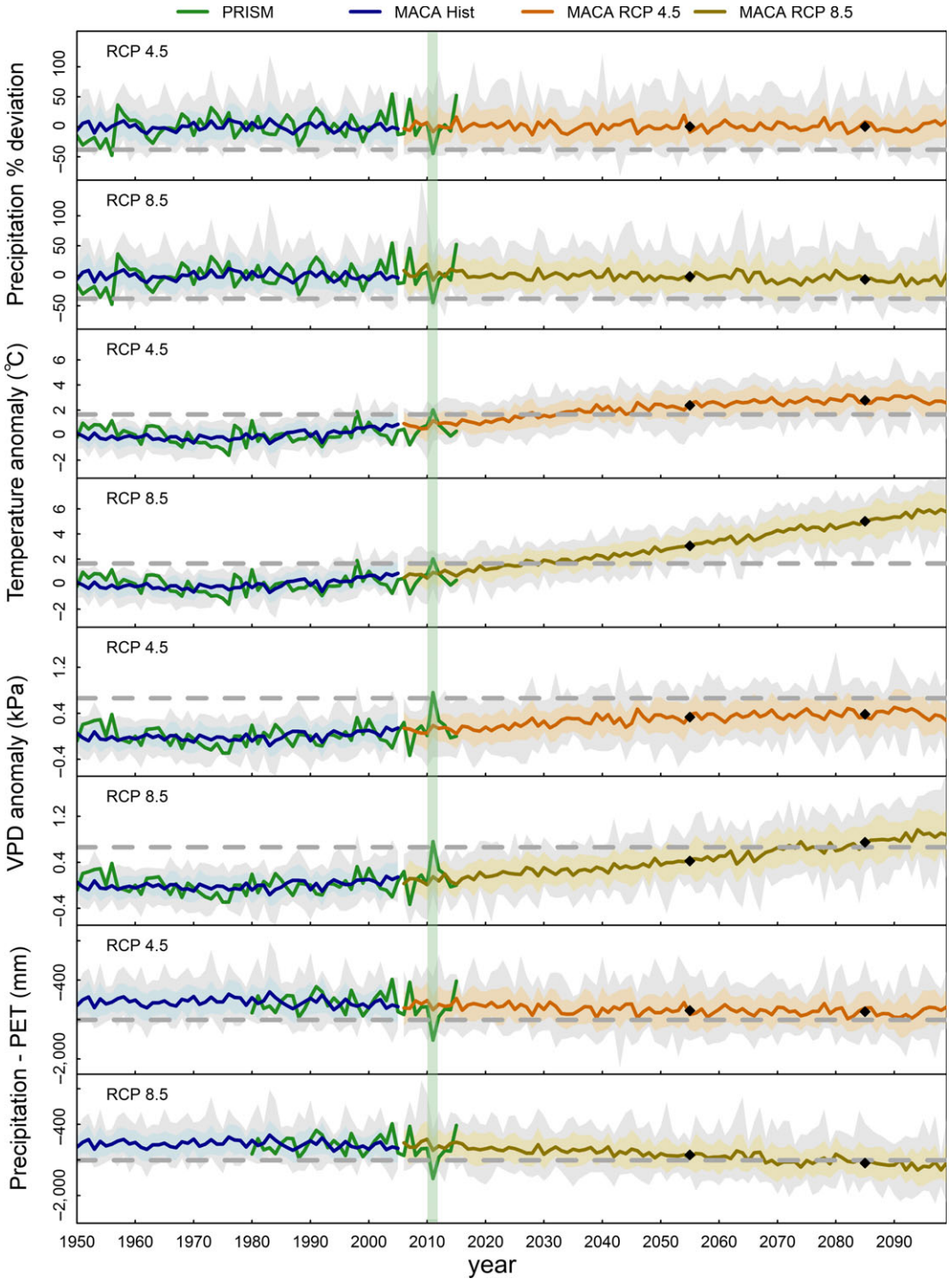

FIGURE 5 Historical and future projections of climate threshold crossings associated with canopy loss: Spatial averages of percent deviation in annual precipitation, anomalies in warm season temperature and vapor pressure deficit (VPD), and annual precipitation minus potential evapotranspiration (PET) for all forested 4-km pixels in Texas. The 2011 drought shown in light green. Climatic thresholds indicated by gray dashed lines, as defined in Fig. 4a. Historical data acquired from PRISM Climate Group (2015) and Abatzoglou (2013). Projected statistically downscaled historical and future MACA climate data an ensemble of 20 GCMs (Abatzoglou & Brown, 2012); solid line: mean, shading: 1 standard deviation, gray shading: range. The first black diamond represents the mean for the period from 2040 to 2069 and the second: 2070 to 2099

mortality was not limited to only semiarid water-limited systems, as was also observed by Allen et al. (2010). Our estimates were corroborated by Texas Forest Service field surveys of observed tree mortality by genus (Moore et al., 2016), which found a ~6.2% loss of trees (stems) and a 7.5% loss of basal area following the 2011 drought. In this study, we did not differentiate canopy loss caused directly from drought vs. indirectly from insects or other pathogens. Many diseases in Texas are more likely to infect water stressed trees

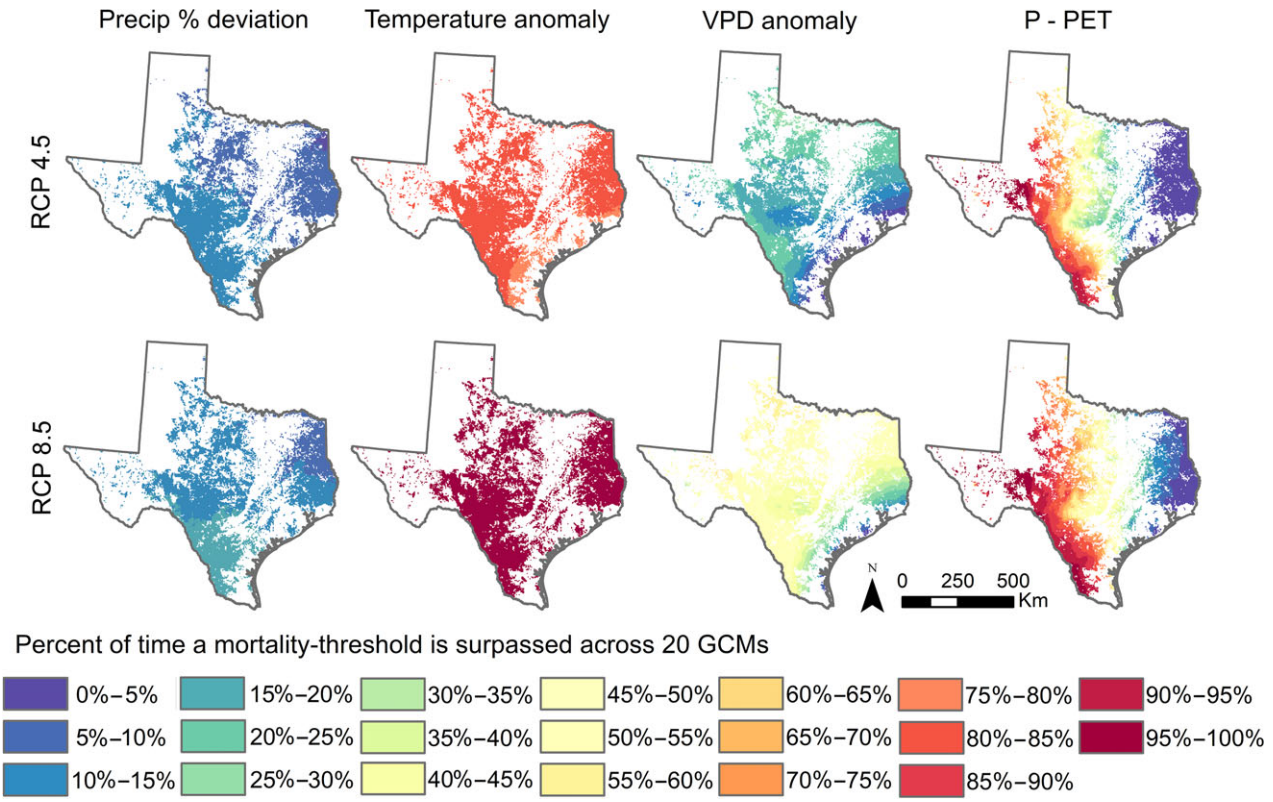

FIGURE 6 Percent of time for which a climate threshold (defined in Figure 4a) was surpassed, considering 20 global climate models (GCMs) over the latter half of the 21st century (2050–2099). For example, if a climate threshold was crossed for 25 years in the 50-year period, for 10 of the 20 GCMs, then this would be represented by an average threshold crossing of 25%. We used statistically downscaled 4-km climate data for Representative Concentration Pathways (RCP) 4.5 and 8.5 scenarios (Abatzoglou & Brown, 2012)

(e.g., in oaks, Hypoxylon canker, *Hypoxylon atropunctatum*, Bassett & Fenn, 1984; and oak wilt, *Ceratocystis fagacearum*, Wilson, 2001; and for pines, Ips bark beetles, Moore et al., 2016), and thus we still considered this drought-induced canopy loss.

Although overall our method was capable of predicting canopy loss across all six modeling zones ranging from closed-canopy forests to open canopy woodlands/shrublands, the approach had some limitations. Underestimation could have occurred in select areas, firstly, because some of the cleared trees we excluded from the analysis could have been dead (e.g., salvage logging). Secondly, regrowth of grass and shrubs under dead canopies can reduce mortality signals (McDowell et al., 2015). Lastly, some studies have observed lagged mortality due to drought (Bigler, Gavin, Gunning, & Veblen, 2007); therefore, trees in Texas may have continued to die, beyond the acquisition date of our postdrought images.

Overestimates of canopy loss in some areas could have also occurred. Firstly, in scaling up to Landsat, some of the predicted mortality could be due to canopy thinning, or partial canopy dieback. In the fine-scale canopy loss maps, we could more accurately distinguish between canopy thinning and dead canopy; therefore, misidentification of canopy thinning as mortality could account for some of the discrepancy between the fine-scale maps and the regional coarse-scale maps. Secondly, to avoid extensive leaf desiccation during drought, many of the trees in Texas can lose their leaves earlier in the season in times of water stress and become "drought-deciduous". We avoided detection of drought-deciduousness across Texas, because we selected postdrought imagery in 2012 instead of in 2011, directly following the drought. It is unlikely that a tree without leaves in 2011 and 2012 would have recovered. However, this was not the case for trees in South Texas, where we did note evidence of full recovery of trees post 2012 (observed in 10 out of 42 orthophotos in South Texas and one out of 29 along the southern edge of the Oakwoods). Postdrought orthophotos used as training data were acquired in 2012; however, postdrought Landsat images used for scaling were acquired in 2013 and 2014. Therefore, if trees recovered post 2012, then the training data would not have captured this recovery. This was likely why the models in South Texas had lower accuracy, particularly in the true positive rate.

Many plant communities were differentially impacted by the drought. Similar to field surveys conducted by the Texas Forest Service in 2012 (Moore et al., 2016), we found that the 2011 drought did not affect all species/ecological systems equally. Specifically, systems dominated by juniper woodlands, pinyon-juniper shrublands, gray oak savanna and woodlands, and post oak woodlands (Figure 7) were most impacted; these systems may be particularly vulnerable to climate change. During the 1950s drought, similar systems were also impacted, including oak (post, spanish, blackjack, and shin) as well as juniper and elm, with particularly high levels of *J. ashei*

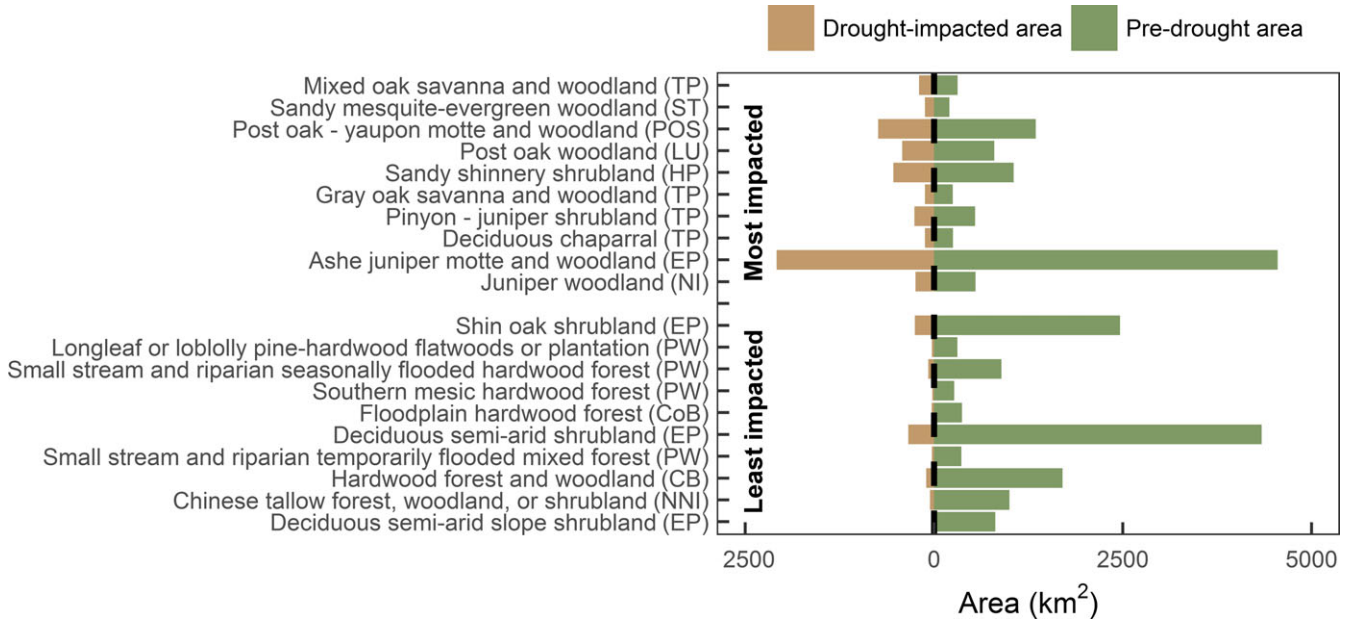

FIGURE 7 The top 10 ecological systems with the highest relative loss (top) and lowest relative loss (bottom), due to the 2011 drought, as quantified through an overlay of our canopy loss maps with an ecological systems map (Elliott et al., 2014). Only ecological systems dominated by trees (231 systems) and with >200 km^2 of area (94 systems) in Texas were considered here. Natural regions in parentheses: TP—Trans Pecos; ST—South Texas; POS—Post Oak Savannah; LU—Llano Uplift; HP—High Plains, EP—Edwards Plateau; NI—Native Invasive; PW—Pineywoods; CoB—Coastal Bend; CB—Columbia Bottomlands; NNI—Non-Native Invasive

mortality in central Texas (Young, 1956). Since the 1950s, *J. ashei*, a woody encroacher, recovered only to be once again killed in large numbers by the 2011 drought. This result would suggest that drought was acting as a control to check the encroachment of *J. ashei*. Other studies, have also found mortality of recently encroached shrubs (Fensham, Fairfax, & Ward, 2009). Future drought events could turn these encroaching shrubs/trees from carbon sinks to carbon sources with substantial consequences to regional carbon cycling (Barger et al., 2011).

Interestingly, much research has focused on pinyon-juniper woodlands dominated by *P. edulis* and *Juniperus* spp of Arizona, New Mexico, and Colorado, where significant tree mortality due to drought and bark beetle occurred, mostly impacting *P. edulis* (Floyd et al., 2009; Mueller et al., 2005). However, less research has focused on drought-induced tree mortality in the pinyon-juniper stands in the Trans Pecos, with different dominant species including *P. cembroides*, *J. deppeana*, *J. pinchotii*, and *J. flaccida* (Moir, 1982). The pinyon-juniper stands of the Trans Pecos also had significant drought-induced canopy loss. A study of the pinyon-juniper stands in Big Bend National Park, found that *P. cembroides* had the highest tree mortality followed by *J. deppeana*, and *Q. emoryi*, resulting from a combined stress of a severe winter freeze event and the 2011 drought (Poulos, 2014). Therefore, within the pinyon-juniper communities of both these regions, the pinyon pine species (e.g., *P. cembroides and P. edulis)* were more vulnerable to drought compared to the juniper species.

In identifying how climate explained spatial patterns of canopy loss across the fivefold precipitation gradient in Texas, we found that canopy loss patterns revealed threshold responses. For example, when either a 1.6°C temperature anomaly, 0.66 kPa VPD anomaly, −38% deviation in precipitation, or −1,206 mm P-PET water deficit were crossed, then canopy loss increased substantially. Although the precipitation threshold was crossed during the 1950s and 2011 droughts, over the past 50 + years the temperature threshold was surpassed for the forested areas of Texas only during 1998 and 2011, and the VPD threshold only in 2011. The temperature threshold was crossed in both 1998 and 2011; however, only in 2011 was there a widespread loss of trees in Texas, which suggests that perhaps these forests were responding more to changes in VPD than temperature. Other studies have also found VPD to be an important climate driver of tree mortality (Breshears et al., 2013; Eamus, Boulain, Cleverly, & Breshears, 2013; Williams et al., 2013; McDowell et al., 2016). VPD is the difference between saturation vapor pressure and actual vapor pressure. Saturation vapor pressure is exponentially related to temperature based on the Clausius-Clapeyron equation and actual vapor pressure is a measure of atmospheric moisture content (Anderson, 1936). The conditions leading to the 2011 VPD anomaly occurred due to a combination of high saturation vapor pressure, attributable to the record high temperatures and the low moisture content in the atmosphere (Williams et al., 2014). For example, atmospheric moisture could increase with rising temperatures to maintain a constant relative humidity. However partly due to limited surface water, models in the southwestern United States do not predict that relative humidity will likely remain constant in the future (Williams et al., 2014). Therefore, VPD is projected to increase with climate change for the southwestern US, both due to increases

in the saturation vapor pressure due to rising temperatures and a minimized increase in atmospheric moisture (Williams et al., 2014).

The 2011 climate conditions were projected to be surpassed on average for the periods from 2040 to 2099 for the temperature anomaly and 2070 to 2099 for both the VPD anomaly and the 2011 P-PET water deficit, under the RCP 8.5 scenario. As these anomalies were projected to become the norm for the latter half of the 21st century, the projected changes could have severe effects on the structure and function of forests in Texas. The ensemble range of 20 GCMs encompassed the variability in historical precipitation; however, the ensemble mean did not, due to buffering that occurred with averaging many models, as other studies in Texas have also noted (Venkataraman, Tummuri, Medina, & Perry, 2016). Therefore, although precipitation projections for the ensemble mean did not cross the precipitation threshold (Figure 5), some of these GCMs individually did project threshold crossings in the future (Figure 6). Additionally, there is still great uncertainty surrounding precipitation and VPD projections of extreme values. Many GCMs do not include regional processes and feedbacks, and thus projections of climate extremes at the regional scale are often less accurate than global trends (Burke, Brown, & Christidis, 2006; Jentsch, Kreyling, & Beierkuhnlein, 2007). Given that future precipitation follows historical observations, atmospheric water demand will increase where temperatures increase; consequently, trees will need to increase evapotranspiration, which could lead to greater water stress (McDowell et al., 2015). This was reflected in the increasingly negative annual P-PET water deficits for the latter half of the 21st century (Figure 5).

There are limitations in defining empirical relationships between climate and spatial patterns of canopy loss. Although climate contributed to these canopy loss patterns, the trends were sometimes variable, indicating that other local-scale factors related to soil, topography, management, and stand density also likely played a role. Moreover defining thresholds that lead to canopy loss is only a first step. The sequence of several drought events can matter more than trends or single events (Miao, Zou, & Breshears, 2009), and the time spent below a threshold can be more significant than the actual threshold crossing for some systems (McDowell et al., 2013). Also, climatic thresholds defined for the 2011 drought may cause more or less tree mortality in the future depending on the ecosystem. For example, a drought may kill vulnerable and poorly adapted trees, with surviving trees remaining on more favorable landscape positions. However, the capacity of a heterogeneous landscape to buffer climate could be overcome if climate extremes are too severe or rapid and if regional climate is coupled to local climate (Hylander, Ehrlen, Luoto, & Meineri, 2015). Also, surviving trees could become more resilient to drought by switching carbon allocation and increasing root or sapwood area at the expense of leaf area (Bréda, Huc, Granier, & Dreyer, 2006), or recovering from declines in hydraulic conductivity through xylem refilling (Meinzer & McCulloh, 2013). Alternatively, surviving trees have the potential to become more vulnerable to future droughts due to xylem dysfunction, such as cavitation fatigue, (Hacke, Stiller, Sperry, Pittermann, & McCulloh, 2001) and reduced carbon reserves (Galiano, Martínez-Vilalta, & Lloret, 2011).

Future research is needed on the recovery of ecosystems following drought, mortality thresholds that incorporate both climate and the environment, and improved projections of extreme climatic events. This study does not quantify recovery following drought. If favorable climates for seedling establishment are never achieved, semiarid communities may fail to recover following a mortality event (Breshears et al., 2005) or differential species recovery may favor species that resprout (Zeppel et al., 2015) and that have more favorable recruitment under global change. Additionally, we only examined how canopy loss related to climatic thresholds. Stronger correlations may exist by incorporating climate and environment, for example by including soil moisture thresholds (Adams et al., 2013). Metrics derived from process-based models (e.g., soil water) have been used to predict future range shifts in western North America (Mathys, Coops, & Waring, 2016). Lastly, improvements are needed for projections of extreme climate conditions in global change models (Bahn, Reichstein, Dukes, Smith, & Mcdowell, 2014), that work at both regional and global scales. Understanding changes in mean climate values can only go so far (Jentsch et al., 2007), as forests are more likely to respond to changes in extremes.

In summary, we mapped drought-induced canopy loss across the state of Texas and documented impacted ecological systems and climate drivers that explained canopy loss patterns across a fivefold precipitation gradient from humid to semiarid regions. Our approach could be used to identify relationships between climate and tree mortality in other semiarid and/or temperate systems experiencing drought. Much of the loss was from *J. ashei*, a recently encroaching shrub/tree. Substantial levels of mortality also occurred for this species during the 1950s drought, suggesting that *J. ashei* was being restricted from further encroachment by drought. Studies have proposed that gains in woody shrub encroachment may counter balance drought-induced forest loss. However, given that woody encroachment seemed to be drought-restricted in this ecosystem, then perhaps less forest loss will be offset than originally thought (Barger et al., 2011). Additionally, we found that the 2011 climate anomalies associated with a 9.5% loss in canopy were likely to become the norm under RCP 8.5 scenario, for the 2011 VPD anomaly and 2011 P-PET water deficit during the 2070–2099 period and for the temperature anomaly during the 2040–2099 period, which could have significant impacts for the forests of Texas. Until more mechanistic approaches can be developed, tested, and parameterized globally, defining empirical relationships between canopy loss and climate may improve our ability to forecast how forests will respond to increased drought pressure following climate change.

ACKNOWLEDGEMENTS

Our funding sources include NASA Earth and Space Science Fellowship (NNX13AN86H), a James B. Duke Fellowship, and United States Department of Agriculture/National Institute of Food and Agriculture (USDA/NIFA) grant (2012-68002-19795). We thank the Texas State

Parks, Texas Master Naturalists, and National Forest Service for providing access to land for field sampling, as well as Chris Edgar and Georgianne Moore for providing summary data from Moore et al. (2016). We also thank Kelly Howell for image processing assistance, and Raven Bier and Evan Williams for field work assistance.

REFERENCES

Abatzoglou, J. T. (2013). Development of gridded surface meteorological data for ecological applications and modelling. *International Journal of Climatology*, *33*, 121–131.

Abatzoglou, J. T., & Brown, T. J. (2012). A comparison of statistical downscaling methods suited for wildfire applications. *International. Journal of Climatology*, *32*, 772–780.

Adams, H. D., Luce, C. H., Breshears, D. D., Allen, C. D., Weiler, M., Hale, V. C., … Huxman, T. E. (2012). Ecohydrological consequences of drought- and infestation- triggered tree die-off : Insights and hypotheses. *Ecohydrology*, *5*, 145–159.

Adams, H. D., Williams, A. P., Xu, C., Rauscher, S. A., Jiang, X., & McDowell, N. G. (2013). Empirical and process-based approaches to climate-induced forest mortality models. *Frontiers in Plant Science*, *4*, 1–5.

AghaKouchak, A., Cheng, L., Mazdiyasni, O., & Farahmand, A. (2014). Global warming and changes in risk of concurrent climate extremes: Insights from the 2014 California drought. *Geophysical Research Letters*, *41*, 8847–8852.

Allen, C. D., Breshears, D. D., & McDowell, N. G. (2015). On underestimation of global vulnerability to tree mortality and forest die-off from hotter drought in the Anthropocene. *Ecosphere*, *6*, 1–55.

Allen, C. D., Macalady, A. K., Chenchouni, H., Bachelet, D., McDowell, N., Vennetier, M., … Cobb, N. (2010). A global overview of drought and heat-induced tree mortality reveals emerging climate change risks for forests. *Forest Ecology and Management*, *259*, 660–684.

Anderegg, W. R. L., Flint, A., Huang, C., Flint, L., Berry, J. A., Davis, F. W., … Field, C. B. (2015). Tree mortality predicted from drought-induced vascular damage. *Nature Geoscience*, *8*, 367–371.

Anderson, D. B. (1936). Relative humidity or vapor pressure deficit. *Ecology*, *17*, 277–283.

Bahn, M., Reichstein, M., Dukes, J. S., Smith, M. D., & Mcdowell, N. G. (2014). Climate-biosphere interactions in a more extreme world. *New Phytologist*, *202*, 356–359.

Baig, M. H. A., Zhang, L., Shuai, T., & Tong, Q. (2014). Derivation of a tasselled cap transformation based on Landsat 8 at-satellite reflectance. *Remote Sensing Letters*, *5*, 423–431.

Barger, N. N., Archer, S. R., Campbell, J. L., Huang, C. Y., Morton, J. A., & Knapp, A. K. (2011). Woody plant proliferation in North American drylands: A synthesis of impacts on ecosystem carbon balance. *Journal of Geophysical Research*, *116*, 1–17.

Bassett, E. N., & Fenn, P. (1984). Latent colonization and pathogenicity of *Hypoxylon atropunctatum* on oaks. *Plant Disease*, *68*, 317–319.

Bigler, C., Gavin, D. G., Gunning, C., & Veblen, T. T. (2007). Drought induces lagged tree mortality in a subalpine forest in the Rocky Mountains. *Oikos*, *116*, 1983–1994.

Bréda, N., Huc, R., Granier, A., & Dreyer, E. (2006). Temperate forest trees and stands under severe drought: a review of ecophysiological responses, adaptation processes and long-term consequences. *Annals of Forest Science*, *63*, 625–644.

Breiman, L. (2001). Random Forests. *Machine Learning*, *45*, 5–32.

Breshears, D. D., Adams, H. D., Eamus, D., McDowell, N. G., Law, D. J., Will, R. E., … Zou, C. B. (2013). The critical amplifying role of increasing atmospheric moisture demand on tree mortality and associated regional die-off. *Frontiers in Plant Science*, *4*, 1–4.

Breshears, D. D., Cobb, N. S., Rich, P. M., Price, K. P., Allen, C. D., Balice, R. G., … Meyer, C. W. (2005). Regional vegetation die-off in response to global-change-type drought. *Proceedings of the National Academy of Sciences of the United States of America*, *102*, 15144–15148.

Burke, E. J., Brown, S. J., & Christidis, N. (2006). Modeling the recent evolution of global drought and projections for the twenty-first century with the hadley centre climate model. *Journal of Hydrometeorology*, *7*, 1113–1125.

Carnicer, J., Coll, M., Ninyerola, M., Pons, X., Sánchez, G., & Peñuelas, J. (2011). Widespread crown condition decline, food web disruption, and amplified tree mortality with increased climate change-type drought. *Proceedings of the National Academy of Sciences of the United States of America*, *108*, 1474–1478.

Ciais, P., Reichstein, M., Viovy, N., Granier, A., Ogée, J., Allard, V., … Valentini, R. (2005). Europe-wide reduction in primary productivity caused by the heat and drought in 2003. *Nature*, *437*, 529–533.

Clifford, M. J., Royer, P. D., Cobb, N. S., Breshears, D. D., & Ford, P. L. (2013). Precipitation thresholds and drought-induced tree die-off: insights from patterns of *Pinus edulis* mortality along an environmental stress gradient. *New Phytologist*, *200*, 413–421.

Cohen, W. B., & Goward, S. N. (2004). Landsat's Role in Ecological Applications of Remote Sensing. *BioScience*, *54*, 535–545.

Comer, P. J., Faber-Langendoen, D., Evans, R. Gawler, S., Josse, C., Kittel, G., … Teague, J. (2003) *Ecological Systems of the United States: A working classification of U.S. terrestrial systems*. Arlington, VA, USA: NatureServe.

Coops, N. C., Johnson, M., Wulder, M. A., & White, J. C. (2006). Assessment of QuickBird high spatial resolution imagery to detect red attack damage due to mountain pine beetle infestation. *Remote Sensing of Environment*, *103*, 67–80.

Crist, E. P. (1985). A TM Tasseled Cap equivalent transformation for reflectance factor data. *Remote Sensing of Environment*, *17*, 301–306.

Daly, C., Smith, J. I., & Olson, K. V. (2015). Mapping atmospheric moisture climatologies across the conterminous United States. *PLoS One*, *10*, 1–33.

De'ath, G., & Fabricius, K. E. (2000). Classification and regression trees: a powerful yet simple technique for ecological data analysis. *Ecology*, *81*, 3178–3192.

Eamus, D., Boulain, N., Cleverly, J., & Breshears, D. D. (2013). Global change-type drought-induced tree mortality: vapor pressure deficit is more important than temperature per se in causing decline in tree health. *Ecology and Evolution*, *3*, 2711–2729.

Elliott, L. F., Diamond, D. D., True, C. D., Blodgett, C. F., Pursell, D., German, D., & Treuer-Kuehn, A. (2014). Ecological mapping systems of Texas: Summary Report. Texas Parks & Wildlife Department, Austin, Texas. Retrieved from: http://tpwd.texas.gov/landwater/land/programs/landscape-ecology/ems/

Fehmi, J. S. (2010). Confusion among three common plant cover definitions may result in data unsuited for comparison. *Journal of Vegetation Science*, *21*, 273–279.

Fensham, R. J., Fairfax, R. J., & Ward, D. P. (2009). Drought-induced tree death in savanna. *Global Change Biology*, *15*, 380–387.

Floyd, M. L., Clifford, M., Cobb, N. S., Hanna, D., Delph, R., Ford, P., & Turner, D. (2009). Relationship of stand characteristics to drought-induced mortality in three Southwestern pinon–juniper woodlands. *Ecological Applications*, *19*, 1223–1230.

Galiano, L., Martínez-Vilalta, J., & Lloret, F. (2011). Carbon reserves and canopy defoliation determine the recovery of Scots pine 4 yr after a drought episode. *New Phytologist*, *190*, 750–759.

Gitelson, A. A., Kaufman, Y. J., & Merzlyak, M. N. (1996). Use of a green channel in remote sensing of global vegetation from EOS-MODIS. *Remote Sensing of Environment*, *58*, 289–298.

González-Roglich, M., & Swenson, J. J. (2016). Tree cover and carbon mapping of Argentine savannas: scaling from field to region. *Remote Sensing of Environment*, *172*, 139–147.

Guardiola-Claramonte, M., Troch, P. A., Breshears, D. D., Huxman, T. E., Switanek, M. B., Durcik, M., & Cobb, N. S. (2011). Decreased

streamflow in semi-arid basins following drought-induced tree die-off: a counter-intuitive and indirect climate impact on hydrology. *Journal of Hydrology*, *406*, 225–233.

Hacke, U. G., Stiller, V., Sperry, J. S., Pittermann, J., & McCulloh, K. A. (2001). Cavitation fatigue. Embolism and refilling cycles can weaken the cavitation resistance of xylem. *Plant physiology*, *125*, 779–786.

Hoerling, M., Kumar, A., Dole, R., Nielsen-Gammon, J. W., Eischeid, J., Perlwitz, J., ... Chen, M. (2013). Anatomy of an extreme event. *Journal of Climate*, *26*, 2811–2832.

Homer, C. G., Dewitz, J. A., Yang, L., Jin, S., Danielson, P., Xian, G., ... Megown, K. (2015). Completion of the 2011 National Land Cover Database for the conterminous United States-Representing a decade of land cover change information. *Photogrammetric Engineering and Remote Sensing*, *81*, 345–354.

Huang, C. Y., & Anderegg, W. R. L. (2012). Large drought-induced aboveground live biomass losses in southern Rocky Mountain aspen forests. *Global Change Biology*, *18*, 1016–1027.

Huete, A. R. (1988). A soil-adjusted vegetation index (SAVI). *Remote Sensing of Environment*, *25*, 295–309.

Hylander, K., Ehrlen, J., Luoto, M., & Meineri, E. (2015). Microrefugia: Not for everyone. *Ambio*, *44*, 60–68.

Ivits, E., Horion, S., Fensholt, R., & Cherlet, M. (2014). Drought footprint on European ecosystems between 1999 and 2010 assessed by remotely sensed vegetation phenology and productivity. *Global Change Biology*, *20*, 581–593.

Jackson, R. B., Randerson, J. T., Canadell, J. G., Anderson, R. G., Avissar, R., Baldocchi, D. D., ... Pataki, D. (2008). Protecting climate with forests. *Environmental Research Letters*, *3*, 44006.

Jentsch, A., Kreyling, J., & Beierkuhnlein, C. (2007). A new generation of climate-change experiments: events, not trends. *Frontiers in Ecology and the Environment*, *5*, 365–374.

Jump, A. S., Mátyás, C., & Peñuelas, J. (2009). The altitude-for-latitude disparity in the range retractions of woody species. *Trends in Ecology and Evolution*, *24*, 694–701.

Liaw, A., & Wiener, M. (2002). Classification and regression by randomForest. *R News*, *2*, 18–22.

Masek, J. G., Vermote, E. F., Saleous, N. E., Wolfe, R., Hall, F. G., Huemmrich, K. F., ... Lim, T. K. (2006). A Landsat Surface Reflectance Dataset for North America, 1990–2000. *IEEE Geoscience and Remote Sensing Letters*, *3*, 68–72.

Mathys, A. S., Coops, N. C., & Waring, R. H. (2016). An ecoregion assessment of projected tree species vulnerabilities in western North America through the 21st century. *Global Change Biology*, *23*, 920–932.

McDowell, N. G., Coops, N. C., Beck, P. S. A., Chambers, J. Q., Gangodagamage, C., Hicke, J. A., ... Allen, C. D. (2015). Global satellite monitoring of climate-induced vegetation disturbances. *Trends in Plant Science*, *20*, 114–123.

McDowell, N. G., Fisher, R. A., Xu, C., Domec, J. C., Hölttä, T., Mackay, D. S., ... Pockman, W. T. (2013). Evaluating theories of drought-induced vegetation mortality using a multimodel-experiment framework. *New Phytologist*, *200*, 304–321.

McDowell, N. G., Williams, A. P., Xu, C., Pockman, W. T., Dickman, L. T., Sevanto, S., ... Koven, C. (2016). Multi-scale predictions of massive conifer mortality due to chronic temperature rise. *Nature Climate Change*, *6*, 295–300.

Meddens, A. J. H., Hicke, J. A., Vierling, L. A., & Hudak, A. T. (2013). Evaluating methods to detect bark beetle-caused tree mortality using single-date and multi-date Landsat imagery. *Remote Sensing of Environment*, *132*, 49–58.

Meinzer, F. C., & McCulloh, K. A. (2013). Xylem recovery from drought-induced embolism: where is the hydraulic point of no return? *Tree physiology*, *33*, 331–334.

Miao, S., Zou, C. B., & Breshears, D. D. (2009). Vegetation responses to extreme hydrological events: sequence matters. *The American Naturalist*, *173*, 113–118.

Michaelian, M., Hogg, E. H., Hall, R. J., & Arsenault, E. (2011). Massive mortality of aspen following severe drought along the southern edge of the Canadian boreal forest. *Global Change Biology*, *17*, 2084–2094.

Mildrexler, D. J., Zhao, M., & Running, S. W. (2009). Testing a MODIS Global Disturbance Index across North America. *Remote Sensing of Environment*, *113*, 2103–2117.

Mitchell, P. J., O'Grady, A. P., Hayes, K. R., & Pinkard, E. A. (2014). Exposure of trees to drought-induced die-off is defined by a common climatic threshold across different vegetation types. *Ecology and Evolution*, *4*, 1088–1101.

Moir, W. H. (1982). A Fire History of the High Chisos, Big Bend National Park, Texas. *Southwestern Association of Naturalists*, *27*, 87–98.

Moore, G. W., Edgar, C. B., Vogel, J. G., Washington-Allen, R. A., March, R. G., & Zehnder, R. (2016). Tree mortality from an exceptional drought spanning mesic to semiarid ecoregions. *Ecological Applications*, *26*, 602–611.

Mueller, R. C., Scudder, C. M., Porter, M. E., Trotter, R. T., Gehring, C. A., & Whitham, T. G. (2005). Differential tree mortality in response to severe drought: evidence for long-term vegetation shifts. *Journal of Ecology*, *93*, 1085–1093.

Norman, S. P., Koch, F. H., & Hargrove, W. W. (2016). Review of broad-scale drought monitoring of forests: Toward an integrated data mining approach. *Forest Ecology and Management*, *380*, 346–358.

Phillips, O. L., van der Heijden, G., Lewis, S. L., Lopez-Gonzalez, G., Aragao, L. E. O. C., Lloyd, J., ... Vilanova, E. (2010). Drought – mortality relationships for tropical forests. *New Phytologist*, *187*, 631–646.

Poulos, H. (2014). Tree mortality from a short-duration freezing event and global-change-type drought in a Southwestern piñon-juniper woodland, USA. *PeerJ*, *2*, e404.

PRISM Climate Group. (2015). *PRISM Gridded Climate Data*. Oregon State University. Retrieved from: http://prism.oregonstate.edu

Qi, J., Chehbouni, A., Huete, A. R., Kerr, Y. H., & Sorooshian, S. (1994). A modified soil adjusted vegetation index. *Remote Sensing of Environment*, *48*, 119–126.

R Core Team. (2015). *R: A language and environment for statistical computing*. Vienna, Austria: R Foundation for Statistical Computing. Retrieved from http://www.r-project.org/

Rind, D., Goldberg, R., Hansen, J., Rosenzweig, C., & Ruedy, R. (1990). Potential evapotranspiration and the likelihood of future drought. *Journal of Geophysical Research*, *95*, 9983–10004.

Ross, R. J., & Elliot, W. P. (1996). Tropospheric water vapor climatology and trends over North America: 1973-93. *Journal of Climate*, *9*, 3561–3574.

Rotenberg, E., & Yakir, D. (2010). Contribution of semi-arid forests to the climate system. *Science*, *327*, 451–454.

Rupp, D. E., Li, S., Massey, N., Sparrow, S. N., Mote, P. W., & Allen, M. (2015). Anthropogenic influence on the changing likelihood of an exceptionally warm summer in Texas, 2011. *Geophysical Research Letters*, *42*, 2392–2400.

Schwantes, A. M., Swenson, J. J., & Jackson, R. B. (2016). Quantifying drought-induced tree mortality in the open canopy woodlands of central Texas. *Remote Sensing of Environment*, *181*, 54–64.

Sing, T., Sander, O., Beerenwinkel, N., & Lengauer, T. (2005). ROCR: visualizing classifier performance in R. *BioInfomatics*, *21*, 3940–3941.

Therneau, T, Atkinson, B, & Ripley, B. (2015). rpart: recursive partitioning and regression trees. R package version 4.1-9.

Tucker, C. J. (1979). Red and photographic infrared linear combinations for monitoring vegetation. *Remote Sensing of Environment*, *8*, 127–150.

US Department of Agriculture. (2014). Geospatial data gateway. Retrieved from http://datagateway.nrcs.usda.gov [March 2014].

USDA Forest Service/U.S. Geological Survey. (2014). MTBS data access: Fire level geospatial data. Retrieved from http://mtbs.gov/dataquery/individualfiredata.html.[Nov 2014].

van Mantgem, P. J., Stephenson, N. L., Byrne, J. C., Daniels, L. D., Franklin, J. F., Fulé, P. Z., ... Veblen, T. T. (2009). Widespread increase of tree mortality rates in the western United States. *Science*, *323*, 521–524.

van Wagtendonk, J. W., Root, R. R., & Key, C. H. (2004). Comparison of AVIRIS and Landsat ETM+ detection capabilities for burn severity. *Remote Sensing of Environment*, *92*, 397–408.

Venkataraman, K., Tummuri, S., Medina, A., & Perry, J. (2016). 21st century drought outlook for major climate divisions of Texas based on CMIP5 multimodel ensemble: implications for water resource management. *Journal of Hydrology*, *534*, 300–316.

Vogelmann, J. E., & Rock, B. N. (1988). Assessing forest damage in high-elevation coniferous forests in Vermont and New Hampshire using thematic mapper data. *Remote Sensing of Environment*, *24*, 227–246.

Vogelmann, J. E., Tolk, B., & Zhu, Z. (2009). Monitoring forest changes in the southwestern United States using multitemporal Landsat data. *Remote Sensing of Environment*, *113*, 1739–1748.

Williams, A. P., Allen, C. D., Macalady, A. K., Griffin, D., Woodhouse, C. A., Meko, D. M., ... McDowell, N. G. (2013). Temperature as a potent driver of regional forest drought stress and tree mortality. *Nature Climate Change*, *3*, 292–297.

Williams, A. P., Seager, R., Berkelhammer, M., Macalady, A. K., Crimmins, M. A., Swetnam, T. W., ... Rahn, T. (2014). Causes and implications of extreme atmospheric moisture demand during the record-breaking 2011 wildfire season in the southwestern United States. *American Meteorological Society*, *53*, 2671–2684.

Wilson, A. D. (2001). Oak wilt: a potential threat to southern and western oak forests. *Journal of Forestry*, *99*, 4–11.

Wilson, E. H., & Sader, S. A. (2002). Detection of forest harvest type using multiple dates of Landsat TM imagery. *Remote Sensing of Environment*, *80*, 385–396.

Young, V. A. (1956). The effect of the 1949-1954 drought on the ranges of Texas. *Journal of Range Managemennt*, *9*, 139–142.

Zeppel, M. J. B., Harrison, S. P., Adams, H. D., Kelley, D. I., Li, G., Tissue, D. T., ... Mcdowell, N. G. (2015). Drought and resprouting plants. *New Phytologist*, *206*, 583–589.

SUPPORTING INFORMATION

Additional Supporting Information may be found online in the supporting information tab for this article.

How to cite this article: Schwantes AM, Swenson JJ, González-Roglich M, Johnson DM, Domec J-C, Jackson RB. Measuring canopy loss and climatic thresholds from an extreme drought along a fivefold precipitation gradient across Texas. *Glob Change Biol*. 2017;00:1–16. https://doi.org/10.1111/gcb.13775